AIAA JOURNAL
Vol. 42, No. 8, August 2004

Branch Switching for Pitchfork Bifurcation in Nonlinear Finite Element Method

M. Jin,* W. Lu,† and Z. B. Bao‡
Northern Jiaotong University, 100044 Beijing, People's Republic of China

A general branch-switching approach is proposed, based on pseudo arc-length continuation in the nonlinear finite element method (FEM), to trace the branch solution curve at the pitchfork bifurcation point in parameter space. By this approach, branch direction can be determined without derivatives of tangent stiffness matrix. This approach is proved mathematically and is inserted into a general FEM code. Stability of equilibrium corresponding to each solution curve is estimated by the Lagrange–Dirichlet criteria. As an example, the whole process of the elastic mode jumping for rectangular thin plates, in which there are many pitchfork bifurcations in parameter space in loading and unloading, is simulated by the improved FEM code.The numerical results are identical with that of an experiment done by previous researchers.

I. Introduction

THE term mode jumping is often used to describe sudden dynamic changes of wave number and mode shape of a buckled structure during quasi-static loading or unloading. Mode jumping can be observed in thin plates. In 1959, Stein[1] presented a buckling experiment on axial-compression plates. During loading, mode shape changes in a violent way and wave number changes from 5 to 6, 6 to 7, 7 to 8 buckles, etc. In 1978, Uemura and Byon[2] did a series of experiments on the secondary buckling of clamped plates under uniaxial compression.

Although numerous analytical studies of the mode jumping for plates have been done,[3−15] the whole process of mode jumping in plates is an open question. When the structure is more complicated, the ways to simulate mode jumping are limited. Because experiments are prohibitively expensive and analytical methods ineffective, the only possible affordable way is to perform computer simulation on the structural mode jumping with the help of the finite element method (FEM) for structure analysis.

In recent years, many authors have paid attention to studies of mode jumping in rectangular plates by nonlinear FEM. Uemura and Byon[2] and Carnoy and Hughes[16] traced numerically the whole solution curve by Newton iteration. Gervais et al.[17] traced the solution path by arc-length continuation and introduced a perturbation to trace branch curve. Wohlever[18] addressed some computational aspects of a group theoretic finite element approach to the buckling and postbuckling analyses of plates. Eriksson et al.[19] introduced an initial imperfection to make a plate snap through in calculation. Stoll and Olson[20] concluded that the instability that initiates the snap occurs not in the vicinity of the initial buckling point, but instead deep in the postbuckling regime. Riks et al.[21] proposed a procedure that consists of the combination of a classical path-following method with a transient integration method. However, up till now, the numerical simulation on the mode-jumping process of a plate has not been perfect.

In this paper, we seek to develop a general-purpose FEM code for the mode jumping of thin walled structures. The first step is the numerical discretization of the nonlinear mechanical model, in which a group of nonlinear algebraic equations with one parameter is formed. For example, the parameter may be a load factor. Generally, the number of nonlinear algebraic equations is very large, greater than several hundreds or several thousands. In solid mechanics, FEM has been used in a successful way for discretization. Now there are geometrically nonlinear models in many general-purpose FEM codes.

The second step is to solve globally the nonlinear algebraic equations with one parameter. In view of differential geometry, unknowns and the parameter construct a high-dimensional space, which is called the parameter space. In the parameter space, the solution of nonlinear algebraic equations with one parameter is a one-dimensional curve, which is called the solution curve. Therefore, the way to solve globally nonlinear algebraic equations with one parameter is to trace a one-dimensional curve in the parameter space. Three problems should be considered as the solution curve is traced numerically: 1) how to treat limit point (tangent bifurcation point, turning point) numerically, at which Newton iteration fails, 2) how to determine the direction of the branch solution curve, which is necessary to trace a new solution curve at pitchfork bifurcation point, and 3) how to estimate numerically stability of equilibrium corresponding to each solution curve.

Arc-length continuation[22] has been used successfully to trace a solution curve with limit points. Many general-purpose FEM codes were developed by arc-length continuation. In this paper, to treat singularity at the limit point, the solution curve is traced by pseudo arc-length continuation, which is a type of arc-length continuation.[22−24]

It is a challenge to solve pitchfork bifurcation by a general FEM code. To the best of our knowledge, there is not a general FEM code by which the pitchfork bifurcation can be treated. Such a general code may be an effective way to solve static bifurcation in structure analysis. First, it is necessary to develop a general approach to treat pitchfork bifurcation. Theoretically, branch switching requires information of derivatives of the tangent stiffness matrix.[24,25] However, it is very difficult to realize the calculation of derivatives of the stiffness matrix in a general FEM code. There are three reasons: 1) If the derivatives of tangent stiffness matrix are formed by the analytical expression for each element, the work is huge because subroutines for every type of element must be improved. 2) Because the error between the difference and derivative of a tangent stiffness matrix is prohibitively large, it is impossible to calculate the derivative of tangent stiffness matrix by finite difference method. 3) Because the derivative of a total tangent stiffness matrix requires much larger memory than a total tangent stiffness matrix in computer, it is impossible to increase such a large amount of memory in a general-purpose FEM code.

To overcome the listed difficulties in branch switching, an approach is proposed by the authors. The approach has the following

Received 27 August 2003; revision received 27 March 2004; accepted for publication 27 March 2004.

*Professor, School of Civil Engineering and Architecture, Institute of Solid Mechanics; jinmingjinming@hotmail.com.
†Professor, School of Computer and Information Technology.
‡Lecturer, School of Computer and Information Technology.

properties: 1) It is suitable for a bifurcation calculation in high-dimensional problems. 2) It is not necessary to calculate derivatives of the tangent stiffness matrix in nonlinear FEM. 3) It has a mathematical proof. 4) There is a geometrical concept of this approach in the parameter space. 5) It is easy to insert this approach into a general FEM code. 6) The CPU time of this approach does not exceed that of solving the total tangent stiffness equations in order. Based on the Lagrange–Dirichlet theorem on stability, a numerical procedure of the stability criterion for nonlinear FEM is given to estimate the stability of equilibrium corresponding to each solution curve.

In Sec. II, the pseudo-arc-length continuation and changing-sign method of detecting pitchfork bifurcation is discussed. Also the difficulty of the branch switching is presented. In Sec. III, an approach to the branch switching problem is proposed, and the mathematical proof is presented. In Sec. IV, convergence of the approximate bifurcation direction in the parameter space is proved mathematically. In Sec. V, a numerical procedure for the stability criterion is described. In Sec. VI, a numerical procedure, which is suitable for a general-purpose FEM code, is given. In Sec. VII, the mode jumping of a rectangular plate in postbuckling is simulated by the improved FEM code. All solution curves near the second bifurcation are given numerically for a clamped support square plate loaded by uniaxial compression. These stable equilibria can simulate the mode jumping of a plate in loading and unloading.

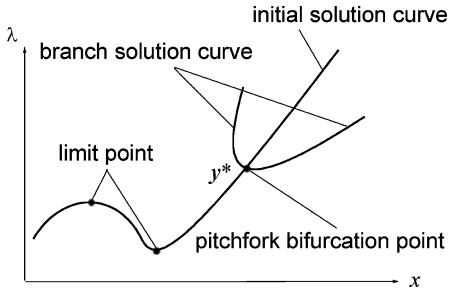

Fig. 1 Scheme of solution curve of Eq. (1).

In Eq. (1), letting

$$\boldsymbol{y} = (\boldsymbol{x}, \lambda)^T \tag{3}$$

where $\boldsymbol{y} = (y_1, y_2, \ldots, y_n, y_{n+1})^T \in R^{n+1}$, we have

$$\hat{\boldsymbol{F}}(\boldsymbol{y}) = \boldsymbol{F}(\boldsymbol{x}, \lambda) = \boldsymbol{0} \tag{4}$$

We define a vector field $\boldsymbol{v}$ in parameter space R^{n+1}

$$\boldsymbol{v}(\boldsymbol{y}) = (J_1, J_2, \ldots, J_{n+1})^T \tag{5}$$

where

$$J_i = \begin{cases} \det\left(\dfrac{\partial \hat{\boldsymbol{F}}}{\partial y_2}, \dfrac{\partial \hat{\boldsymbol{F}}}{\partial y_3}, \ldots, \dfrac{\partial \hat{\boldsymbol{F}}}{\partial y_{n+1}}\right), & i = 1 \\ (-1)^{i+1} \det\left(\dfrac{\partial \hat{\boldsymbol{F}}}{\partial y_1}, \ldots, \dfrac{\partial \hat{\boldsymbol{F}}}{\partial y_{i-1}}, \dfrac{\partial \hat{\boldsymbol{F}}}{\partial y_{i+1}}, \ldots, \dfrac{\partial \hat{\boldsymbol{F}}}{\partial y_{n+1}}\right), & i = 2, \ldots, n \\ (-1)^{n+2} \det\left(\dfrac{\partial \hat{\boldsymbol{F}}}{\partial y_1}, \dfrac{\partial \hat{\boldsymbol{F}}}{\partial y_2}, \ldots, \dfrac{\partial \hat{\boldsymbol{F}}}{\partial y_n}\right), & i = n+1 \end{cases}$$

II. Pseudo-Arc-Length Continuation, Changing-Sign Method, and Difficulty of Branch Switching

A. Pseudo-Arc-Length Continuation

Consider the following nonlinear algebraic equations:

$$\boldsymbol{F}(\boldsymbol{x}, \lambda) = \boldsymbol{0} \tag{1}$$

where mapping $\boldsymbol{F}: R^{n+1} \to R^n$, vector $\boldsymbol{x} \in R^n$ is unknown, and $\lambda \in R^1$ is a parameter. In geometrically nonlinear FEM, vector $\boldsymbol{x}$ is the nodal displacements, λ is load factor, and Eq. (1) is the equilibrium equation. The solution of Eq. (1) is a one-dimension curve in parameter space R^{n+1}.

Three problems should be considered: 1) tracing solution curve of Eq. (1) numerically, 2) recognizing singular point and determining position of singular point in parameter space R^{n+1}, and 3) branch switching at the pitchfork bifurcation point.

By Newton iteration, Eq. (1) is transformed into the Cauchy problem:

$$\dot{\boldsymbol{x}}(\lambda) = -[D_x \boldsymbol{F}(\boldsymbol{x}, \lambda)]^{-1} D_\lambda \boldsymbol{F}(\boldsymbol{x}, \lambda)$$
$$\boldsymbol{x}(0) = \boldsymbol{x}_0 \tag{2}$$

where $\dot{\boldsymbol{x}}(\lambda) = \mathrm{d}\boldsymbol{x}/\mathrm{d}\lambda$, matrix $D_x\boldsymbol{F}$ denotes partial derivatives of $\boldsymbol{F}$ to $\boldsymbol{x}$, and $D_\lambda \boldsymbol{F}$ denotes partial derivatives of $\boldsymbol{F}$ to λ. In geometrically nonlinear FEM, $D_x\boldsymbol{F}$ and $D_\lambda \boldsymbol{F}$ are the tangent stiffness matrix and the unit loading vector, respectively.

In Eq. (2), we can see that as long as matrix $D_x\boldsymbol{F}$ is nonsingular, the solution curve $\boldsymbol{x} = \boldsymbol{x}(\lambda)$ can be traced by Newton iteration. However, Newton iteration fails at a singular point where matrix $D_x\boldsymbol{F}$ is singular. For example, matrix $D_x\boldsymbol{F}$ is singular at the limit point on the solution curve as shown in Fig. 1. Arc-length continuation[22–24] can trace a solution curve through the limit point. Pseudo-arc-length continuation, which is a kind of arc-length continuation, is used in this paper. Pseudo-arc-length continuation is described as follows.

If $\boldsymbol{y}$ is a solution of Eq. (1) or (4), then the vector $\boldsymbol{v}(\boldsymbol{y}) \in R^{n+1}$ is the tangential direction at point $\boldsymbol{y}$ on the solution curve. Thus, vector $\boldsymbol{v}$ on the solution curve is called the tangential vector of the solution curve.

Pseudo-arc-length continuation has two steps:

1) Euler prediction

$$\boldsymbol{y}_k = \boldsymbol{y}_{k-1} + \boldsymbol{\tau}(\boldsymbol{y}_{k-1})(s_k - s_{k-1}) \qquad (k = 1, 2, \ldots) \tag{6}$$

where $\boldsymbol{y}_{k-1}$ is a known point on the solution curve, $\boldsymbol{\tau}$ is the unit vector of $\boldsymbol{v}$ at $\boldsymbol{y}_{k-1}$, that is, $\boldsymbol{\tau} = \boldsymbol{v}/\|\boldsymbol{v}\|$, $(s_k - s_{k-1})$ is the arc length of the kth step, and $\boldsymbol{y}_k$ is an Euler prediction point.

2) Newton correction

$$\boldsymbol{y}_k^0 = \boldsymbol{y}_k$$
$$\boldsymbol{y}_k^l = \boldsymbol{y}_k^{l-1} - \begin{bmatrix} D\hat{\boldsymbol{F}}(\boldsymbol{y}_k) \\ \boldsymbol{\tau}^T(\boldsymbol{y}_k) \end{bmatrix}^{-1} \begin{bmatrix} \hat{\boldsymbol{F}}\left(\boldsymbol{y}_k^{l-1}\right) \\ 0 \end{bmatrix} \qquad (l = 1, 2, \ldots) \tag{7}$$

where matrix $D\hat{\boldsymbol{F}}(\boldsymbol{y}_k)$ is the derivative of $\hat{\boldsymbol{F}}$ to $\boldsymbol{y}_k$.

As long as $\boldsymbol{v}(\boldsymbol{y}_k) \neq 0$ and $\boldsymbol{y}_k$ is near the solution curve, the sequence $\boldsymbol{y}_k^0, \boldsymbol{y}_k^1, \boldsymbol{y}_k^2, \ldots$ in the Newton correction (7) converges to another point $\bar{\boldsymbol{y}}_k$ on the solution curve.

Because $\mathrm{rank}(D_x\boldsymbol{F}) = n - 1$ and $\mathrm{rank}(D_x\boldsymbol{F}, D_\lambda\boldsymbol{F}) = n$ at the limit point, vector $\boldsymbol{v}$ is a nonzero vector. Because

$$\det\begin{pmatrix} D\hat{\boldsymbol{F}} \\ \boldsymbol{\tau}^T \end{pmatrix} = \|\boldsymbol{v}\|$$

matrix

$$\begin{pmatrix} D\hat{\boldsymbol{F}} \\ \boldsymbol{\tau}^T \end{pmatrix}$$

is nonsingular at the limit point. Therefore, the pseudo-arc-length continuation can trace the solution curve through the limit point.

If we calculate $\boldsymbol{v}$ directly by Eq. (5), the error of the numerical results is great for large n. However, the direction of $\boldsymbol{v}$, namely, unit vector $\boldsymbol{\tau}$, can be calculated accurately by numerical procedure (Sec. VI.A).

B. Changing-Sign Method

When $\text{rank}[D_x\boldsymbol{F}, D_\lambda\boldsymbol{F}] < n$, point $(\boldsymbol{x}, \lambda)$ may be a pitchfork bifurcation point in the parameter space R^{n+1} as shown in Fig. 1. At the pitchfork bifurcation point, the solution of Eq. (1) begins to bifurcate with the change of λ.

There are two kinds of pitchfork bifurcations: simple bifurcation and multibifurcation. Point $(\boldsymbol{x}, \lambda)$ is called the simple-bifurcation point if $\text{rank}(D_x\boldsymbol{F}, D_\lambda\boldsymbol{F}) = n-1$. Point $(\boldsymbol{x}, \lambda)$ is called the multibifurcation point if $\text{rank}(D_x\boldsymbol{F}, D_\lambda\boldsymbol{F}) < n-1$. In this paper, we consider only the simple-bifurcation point. There is a theorem for the simple-bifurcation point.

Theorem 1: If tangential vector $\boldsymbol{v}$ inverses its direction between point $\boldsymbol{a}$ and $\boldsymbol{b}$ on the solution curve, namely,

$$\text{sgn}(v_i|_a) + \text{sgn}(v_i|_b) = 0 \qquad (i = 1, 2, \ldots, n+1) \tag{8}$$

then there is a pitchfork bifurcation point between point $\boldsymbol{a}$ and $\boldsymbol{b}$ on the solution curve. In Eq. (8), $v_i|_a$ and $v_i|_b$ are the components of tangential vector $\boldsymbol{v}$ at point $\boldsymbol{a} \in R^{n+1}$ and point $\boldsymbol{b} \in R^{n+1}$ on the solution curve, respectively. Therefore, $\boldsymbol{\tau}^T(\boldsymbol{a})\boldsymbol{\tau}(\boldsymbol{b}) < 0$ is a necessary condition for there to be a pitchfork bifurcation point on the solution curve between point $\boldsymbol{a}$ and $\boldsymbol{b}$, where vector $\boldsymbol{\tau}$ is the unit vector of $\boldsymbol{v}$. This method of detecting pitchfork bifurcation point is called the changing-sign method and is used in this paper.

C. Difficulty of Branch Switching

As a pitchfork bifurcation point is detected on the solution curve, there is a new solution curve, which is called the branch solution curve, as shown in Fig. 1. The old solution curve is called the initial solution curve. By arc-length continuation equations (6) and (7), it is necessary to know the tangential direction of each branch solution curve at the pitchfork bifurcation point. In other words, we must know the tangential vector $\boldsymbol{\tau}$ for each branch solution curve. The procedure of calculating the tangential direction of each branch solution curve is called branch switching.

Suppose $\boldsymbol{y}^*$ denotes a bifurcation point as shown in Fig. 1. $D\boldsymbol{v}(\boldsymbol{y}^*)$ denotes the derivative of $\boldsymbol{v}$ to $\boldsymbol{y}$ at $\boldsymbol{y}^*$, that is,

$$D\boldsymbol{v}(\boldsymbol{y}^*) = \begin{pmatrix} \dfrac{\partial J_1}{\partial y_1} & \dfrac{\partial J_2}{\partial y_1} & \cdots & \dfrac{\partial J_{n+1}}{\partial y_1} \\ \cdots & & & \\ \dfrac{\partial J_1}{\partial y_{n+1}} & \dfrac{\partial J_2}{\partial y_{n+1}} & \cdots & \dfrac{\partial J_{n+1}}{\partial y_{n+1}} \end{pmatrix}, \qquad \text{at} \quad \boldsymbol{y} = \boldsymbol{y}^* \tag{9}$$

Let

$$\boldsymbol{A} = (\boldsymbol{\Phi}_1, \boldsymbol{\Phi}_2)^T D\boldsymbol{v}(\boldsymbol{y}^*)(\boldsymbol{\Phi}_1, \boldsymbol{\Phi}_2) \tag{10}$$

where $\boldsymbol{\Phi}_1 \in R^{n+1}$ and $\boldsymbol{\Phi}_2 \in R^{n+1}$ are bases of the null space $N[D\hat{\boldsymbol{F}}(\boldsymbol{y}^*)] = \text{span}(\boldsymbol{\Phi}_1, \boldsymbol{\Phi}_2)$, $\|\boldsymbol{\Phi}_1\| = \|\boldsymbol{\Phi}_2\| = 1$, and $\boldsymbol{\Phi}_1^T\boldsymbol{\Phi}_2 = 0$. The directions of the initial solution curve and the branch solution curve at the pitchfork bifurcation point are given theoretically by the following theorem.

Theorem 2: If there are two nontrivial real different eigenvalues in $\boldsymbol{A}\boldsymbol{\xi} = \mu\boldsymbol{\xi}$, where matrix $\boldsymbol{A}$ is defined in Eq. (10), then the direction of the initial solution curve and the branch solution curve is

$$\boldsymbol{u}^i = (\boldsymbol{\Phi}_1, \boldsymbol{\Phi}_2)\boldsymbol{\xi}^i \qquad (i = 1, 2) \tag{11}$$

where vector $\boldsymbol{\xi}^i \in R^2$ is the eigenvector of matrix $\boldsymbol{A}$.

Between $\boldsymbol{u}^1$ and $\boldsymbol{u}^2$, one is the tangential direction of the initial solution curve, and the other is the tangential direction of the branch solution curve. In Eq. (11), $\boldsymbol{u}^1$ and $\boldsymbol{u}^2$ are the exact tangential directions of the initial solution curve and the tangential direction of the branch solution curve as shown in Fig. 2.

In nonlinear FEM, it is difficult to calculate $\boldsymbol{u}^1$ and $\boldsymbol{u}^2$ from Eq. (11) because $\boldsymbol{u}^1$ and $\boldsymbol{u}^2$ are determined by matrix $\boldsymbol{A}$ in Eq. (10).

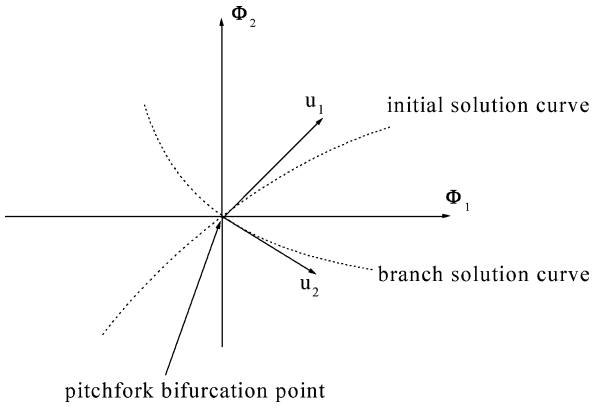

Fig. 2 Bifurcation direction on null space $N[D\hat{\boldsymbol{F}}(\boldsymbol{y}^*)]$.

Matrix $\boldsymbol{A}$ is determined by matrix $D\boldsymbol{v}$ in Eq. (9). Matrix $D\boldsymbol{v}$ is determined by $\partial J_i/\partial y_j$, $i, j = 1, 2, \ldots, n+1$. In Eq. (5), we can see that $\partial J_i/\partial y_j$ is determined by $\partial^2\hat{\boldsymbol{F}}/\partial y_k\partial y_j, k = 1, 2, \ldots, n+1$. In Eqs. (3) and (4), we can see that $\partial^2\hat{\boldsymbol{F}}/\partial y_k\partial y_j$ is determined by $(\partial/\partial\boldsymbol{x})(D_x\boldsymbol{F})$. Thus, we had to calculate $(\partial/\partial\boldsymbol{x})(D_x\boldsymbol{F})$.

In geometrically nonlinear FEM, matrix $D_x\boldsymbol{F} \in R^n \times R^n$ is the total tangent stiffness matrix of the structure and is the assembly of the element tangent stiffness matrix. To calculate $(\partial/\partial\boldsymbol{x})(D_x\boldsymbol{F})$, we had to give the analytical expression of the derivative of the element tangent stiffness matrix to the nodal displacement. Therefore, we had to do an element analysis again. To improve an existing general FEM code, the workload of an element analysis is huge. This is one of the reasons why it is difficult to calculate $\boldsymbol{u}^1$ and $\boldsymbol{u}^2$ from Eq. (11).

On the other hand, even if we have the numerical results of $\partial^2\hat{\boldsymbol{F}}/\partial y_j\partial y_k$, we are not able to calculate $\partial J_i/\partial y_k$ in Eq. (9) numerically because

$$\frac{\partial J_i}{\partial y_k} = (-1)^{i+1}\sum_{l\neq i}^{n+1}\det\left(\frac{\partial\hat{\boldsymbol{F}}}{\partial y_1}, \ldots, \frac{\partial^2\hat{\boldsymbol{F}}}{\partial y_l\partial y_k}, \ldots, \frac{\partial\hat{\boldsymbol{F}}}{\partial y_{i-1}}, \frac{\partial\hat{\boldsymbol{F}}}{\partial y_{i+1}}, \ldots, \frac{\partial\hat{\boldsymbol{F}}}{\partial y_{n+1}}\right) \tag{12}$$

and numerical calculation for the determinant

$$\det\left(\frac{\partial\hat{\boldsymbol{F}}}{\partial y_1}, \ldots, \frac{\partial^2\hat{\boldsymbol{F}}}{\partial y_l\partial y_k}, \ldots, \frac{\partial\hat{\boldsymbol{F}}}{\partial y_{i-1}}, \frac{\partial\hat{\boldsymbol{F}}}{\partial y_{i+1}}, \ldots, \frac{\partial\hat{\boldsymbol{F}}}{\partial y_{n+1}}\right) \tag{13}$$

are impossible where n is a very large number, for example, $n > 1000$, in geometrically nonlinear FEM. Therefore, it is necessary to develop a new approach for determining bifurcation direction.

III. Branch-Switching Approach

Here, $\boldsymbol{y}^*$ denotes the simple-bifurcation point on a solution curve, namely, $\hat{\boldsymbol{F}}(\boldsymbol{y}^*) = 0$, $\boldsymbol{v}(\boldsymbol{y}^*) = \boldsymbol{0}$, and $\text{rank}[D\hat{\boldsymbol{F}}(\boldsymbol{y}^*)] = n-1$. Suppose $N[D\hat{\boldsymbol{F}}(\boldsymbol{y}^*)] = \text{span}(\boldsymbol{\Phi}_1, \boldsymbol{\Phi}_2)$, where $\boldsymbol{\Phi}_1, \boldsymbol{\Phi}_2 \in R^{n+1}$, $\|\boldsymbol{\Phi}_1\| = \|\boldsymbol{\Phi}_2\| = 1$, and $\boldsymbol{\Phi}_1^T\boldsymbol{\Phi}_2 = 0$. We suppose that $\boldsymbol{y}^*$ is an isolated singular point on null space $N[D\hat{\boldsymbol{F}}(\boldsymbol{y}^*)]$, that is,

$$\text{rank}[D\hat{\boldsymbol{F}}(\boldsymbol{y}^*)] = n-1, \qquad \text{rank}\lfloor D\hat{\boldsymbol{F}}(\boldsymbol{y}^* + \Delta\boldsymbol{y})\rfloor = n \tag{14}$$

where $\Delta\boldsymbol{y} \neq \boldsymbol{0}$ and $\Delta\boldsymbol{y} \in \text{span}\,(\boldsymbol{\Phi}_1, \boldsymbol{\Phi}_2)$. Let

$$\Delta\boldsymbol{y} = \varepsilon(\boldsymbol{\Phi}_1\cos\theta + \boldsymbol{\Phi}_2\sin\theta) \tag{15}$$

where $\varepsilon > 0$ and $\theta \in [-\pi, \pi]$ are unknown. Let

$$\boldsymbol{T} = -\boldsymbol{\Phi}_1\sin\theta + \boldsymbol{\Phi}_2\cos\theta \tag{16}$$

If $\boldsymbol{y}^* + \Delta\boldsymbol{y}$ is close to the branch solution curve, $\Delta\boldsymbol{y}$ is an approximate tangential direction of the branch solution curve. Then

the branch solution curve can be traced by the pseudo-arc-length continuation. By Theorem 3, θ can be determined so that $\boldsymbol{y}^* + \Delta\boldsymbol{y}$ is close to the initial solution curve or the branch solution curve. Theorem 3 is proposed by the authors.

Theorem 3: If $D\hat{\boldsymbol{F}}(\boldsymbol{y}^* + \Delta\boldsymbol{y})\Delta\boldsymbol{y} = \boldsymbol{0} \in R^{n+1}$, then $\boldsymbol{v}^T(\varepsilon, \theta)\boldsymbol{T}(\theta) = \boldsymbol{0} \in R^1$.

Proof: Let $D\hat{\boldsymbol{F}}(\boldsymbol{y}^* + \Delta\boldsymbol{y}) = (\boldsymbol{B}_1, \ldots, \boldsymbol{B}_{n+1})$, where

$$\boldsymbol{B}_i = \left.\frac{\partial \hat{\boldsymbol{F}}}{\partial \boldsymbol{y}_i}\right|_{y^* + \Delta y} \in R^n, \qquad i = 1, \ldots, n+1$$

Because point $\boldsymbol{y}^*$ is an isolated singular point on null space $N[D\hat{\boldsymbol{F}}(\boldsymbol{y}^*)]$,

$$\Delta\boldsymbol{y} = \varepsilon(\boldsymbol{\Phi}_1 \cos\theta + \boldsymbol{\Phi}_2 \sin\theta) \in N[D\hat{\boldsymbol{F}}(\boldsymbol{y}^*)]$$

$$\Delta\boldsymbol{y} \neq \boldsymbol{0}$$

Therefore, $\boldsymbol{v}(\boldsymbol{y}^* + \Delta\boldsymbol{y}) \neq \boldsymbol{0}$.

Namely, $\exists k \in S$, where set $S = (l | l = 1, \ldots, n+1)$, k makes

$$J_k = (-1)^{k+1} \det(\boldsymbol{B}_1, \ldots, \boldsymbol{B}_{k-1}, \boldsymbol{B}_{k+1}, \ldots, \boldsymbol{B}_{n+1}) \neq 0 \quad (17)$$

Equation $D\hat{\boldsymbol{F}}(\boldsymbol{y}^* + \Delta\boldsymbol{y})\Delta\boldsymbol{y} = \boldsymbol{0}$ can be written in matrix form

$$(\boldsymbol{B}_1, \ldots, \boldsymbol{B}_k, \ldots, \boldsymbol{B}_{n+1}) \begin{pmatrix} \Delta y_1 \\ \vdots \\ \Delta y_k \\ \vdots \\ \Delta y_{n+1} \end{pmatrix} = \boldsymbol{0} \quad (18)$$

Equation (18) is equivalent to

$$(\boldsymbol{B}_1, \ldots, \boldsymbol{B}_{k-1}, \boldsymbol{B}_{k+1}, \ldots, \boldsymbol{B}_{n+1}) \begin{pmatrix} \Delta y_1 \\ \vdots \\ \Delta y_{k-1} \\ \Delta y_{k+1} \\ \vdots \\ \Delta y_{n+1} \end{pmatrix} = \boldsymbol{B}_k(-\Delta y_k) \quad (19)$$

Considering Eq. (17), we have

$$\det(\boldsymbol{B}_1, \ldots, \boldsymbol{B}_{k-1}, \boldsymbol{B}_{k+1}, \ldots, \boldsymbol{B}_{n+1}) \neq 0 \quad (20)$$

By the Cramer rule, we have the solution of Eq. (19):

$$\Delta y_j = \frac{\det(\boldsymbol{B}_1, \ldots, \boldsymbol{B}_{k-1}, \boldsymbol{B}_{k+1}, \ldots, \boldsymbol{B}_{j-1}, \boldsymbol{B}_k, \boldsymbol{B}_{j+1}, \ldots, \boldsymbol{B}_{n+1})}{\det(\boldsymbol{B}_1, \ldots, \boldsymbol{B}_{k-1}, \boldsymbol{B}_{k+1}, \ldots, \boldsymbol{B}_{n+1})} \times(-\Delta y_k), \ (j \neq k) \quad (21)$$

Equation (21) can be written as

$$\Delta y_j = \frac{(-1)^{j-k-1} \det(\boldsymbol{B}_1, \ldots, \boldsymbol{B}_{j-1}, \boldsymbol{B}_{j+1}, \ldots, \boldsymbol{B}_{n+1})}{\det(\boldsymbol{B}_1, \ldots, \boldsymbol{B}_{k-1}, \boldsymbol{B}_{k+1}, \ldots, \boldsymbol{B}_{n+1})}(-\Delta y_k) = \frac{J_j}{J_k}\Delta y_k \qquad (j \neq k) \quad (22)$$

When $\Delta y_k = (J_k/J_k)\Delta y_k$ and Eq. (5) are considered, Eq. (22) can be written as

$$\Delta\boldsymbol{y} = (\Delta y_k / J_k)\boldsymbol{v} \quad (23)$$

If $\Delta\boldsymbol{y}_k = 0$ in Eq. (23), then $\Delta\boldsymbol{y} = \boldsymbol{0}$. Because $\Delta\boldsymbol{y} = 0$ contradicts Eq. (15), $\Delta y_k \neq 0$. Equation (23) can be written as

$$\boldsymbol{v} = (J_k/\Delta y_k)\Delta\boldsymbol{y} \quad (24)$$

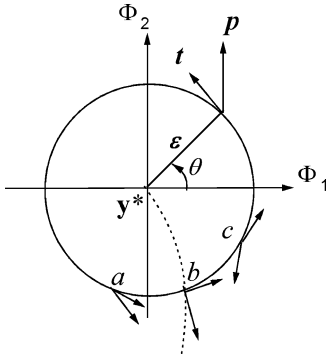

Fig. 3 Projection of $\boldsymbol{v}$ and $\boldsymbol{T}$ in the null space.

Substituting Eq. (15) into Eq. (24) and considering Eq. (16), we have

$$\boldsymbol{v}^T\boldsymbol{T} = (J_k/\Delta y_k)\varepsilon\left(\boldsymbol{\Phi}_1^T \cos\theta + \boldsymbol{\Phi}_2^T \sin\theta\right)(-\boldsymbol{\Phi}_1 \sin\theta + \boldsymbol{\Phi}_2 \cos\theta) \quad (25)$$

Substituting $\|\boldsymbol{\Phi}_1\| = \|\boldsymbol{\Phi}_2\| = 1$ and $\boldsymbol{\Phi}_1^T\boldsymbol{\Phi}_2 = 0$ into Eq. (25), we have $\boldsymbol{v}^T\boldsymbol{T} = 0$. □

There is a geometrical concept in Theorem 3. In parameter space R^{n+1}, null space $N[D\hat{\boldsymbol{F}}(\boldsymbol{y}^*)] = \text{span}(\boldsymbol{\Phi}_1, \boldsymbol{\Phi}_2)$ is the tangential plane of the initial solution curve and branch solution curve at bifurcation point $\boldsymbol{y}^*$. On this tangential plane, the locus of $\boldsymbol{y}^* + \Delta\boldsymbol{y}$, where $\Delta\boldsymbol{y}$ is defined in Eq. (15), is a circle with center $\boldsymbol{y}^*$ and radius ε as shown in Fig. 3. The approximate solution of Eq. (1) or Eq. (4) on the circle makes $\boldsymbol{v}^T(\varepsilon, \theta)\boldsymbol{T}(\theta) = 0 \in R^1$. Because the Taylor expansion of $\hat{\boldsymbol{F}}(\boldsymbol{y}^*)$ at point $\boldsymbol{y}^* + \Delta\boldsymbol{y}$ is

$$\hat{\boldsymbol{F}}(\boldsymbol{y}^*) = \hat{\boldsymbol{F}}(\boldsymbol{y}^* + \Delta\boldsymbol{y}) - D\hat{\boldsymbol{F}}(\boldsymbol{y}^* + \Delta\boldsymbol{y})\Delta\boldsymbol{y} + o(\|\Delta\boldsymbol{y}\|) \quad (26)$$

where $\hat{\boldsymbol{F}}(\boldsymbol{y}^*) = \boldsymbol{0}$, we have

$$\hat{\boldsymbol{F}}(\boldsymbol{y}^* + \Delta\boldsymbol{y}) = D\hat{\boldsymbol{F}}(\boldsymbol{y}^* + \Delta\boldsymbol{y})\Delta\boldsymbol{y} - o(\|\Delta\boldsymbol{y}\|) \quad (27)$$

in the null space. Thus, the zero point of $D\hat{\boldsymbol{F}}(\boldsymbol{y}^* + \Delta\boldsymbol{y})\Delta\boldsymbol{y}$ is an approximate zero point of $\hat{\boldsymbol{F}}(\boldsymbol{y}^* + \Delta\boldsymbol{y})$ because radius ε is small enough. At the approximate zero point, vector $\boldsymbol{v}$ is parallel with the radius of the circle and vertical to the tangent of the circle at the same point, namely, $\boldsymbol{v}^T T = 0$, as shown in Fig. 3.

The projection of vector $\boldsymbol{v}$ on the tangential plane is

$$\boldsymbol{p}(\varepsilon, \theta) = \begin{pmatrix} \boldsymbol{\Phi}_1^T \\ \boldsymbol{\Phi}_2^T \end{pmatrix} \boldsymbol{v}\left[\boldsymbol{y}^* + \varepsilon(\boldsymbol{\Phi}_1 \cos\theta + \boldsymbol{\Phi}_2 \sin\theta)\right] \quad (28)$$

where $\boldsymbol{p} \in R^2$. The projection of vector $\boldsymbol{T}$ in Eq. (16) on the tangential plane can be written as

$$\boldsymbol{t}(\theta) = \begin{pmatrix} \boldsymbol{\Phi}_1^T \\ \boldsymbol{\Phi}_2^T \end{pmatrix} \boldsymbol{T} \quad (29)$$

where $\boldsymbol{t} \in R^2$.

From Eqs. (28) and (29), we have

$$\boldsymbol{v}^T\boldsymbol{T} = \boldsymbol{p}^T\boldsymbol{t} \quad (30)$$

In Fig. 3, $\boldsymbol{p}^T\boldsymbol{t}$ (or $\boldsymbol{v}^T\boldsymbol{T}$) is greater than, equal to, and less than zero, corresponding to points a, b, and c on the circle, respectively. Point b is an approximate point of a solution curve. In other words, point b is one of the nearest points to a solution curve on the circle. The dotted line is a projection of a solution curve on the tangential plane $N[D\hat{\boldsymbol{F}}(\boldsymbol{y}^*)]$.

If the bifurcation point $\boldsymbol{y}^*$ is known and a suitable ε is given, θ can be determined by the equation

$$\boldsymbol{v}^T(\varepsilon, \theta)\boldsymbol{T}(\theta) = 0 \in R^1 \quad (31)$$

After θ is determined, we have an approximate bifurcation direction $\boldsymbol{v}(\varepsilon, \theta) \in R^{n+1}$ in the parameter space R^{n+1}. The numerical procedure for solving Eq. (31) is presented in Sec. VI.D.

IV. Convergence of the Approximate Bifurcation Direction

The approximate bifurcation direction θ in Eq. (31) is related to ε. In view of the numerical calculation, it should be that the smaller ε is, the more accurate the approximate bifurcation direction $\Delta \boldsymbol{y}$ is. In other words, as radius $\varepsilon \to 0$, the approximate bifurcation directions determined by Eq. (31) converge to the exact bifurcation direction $\boldsymbol{u}^1$ and $\boldsymbol{u}^2$ in Theorem 2. This kind of convergence for the approximate bifurcation direction can be proved.

Theorem 4: Suppose $A = (\boldsymbol{\Phi}_1, \boldsymbol{\Phi}_2)^T D\boldsymbol{v}(\boldsymbol{y}^*)(\boldsymbol{\Phi}_1, \boldsymbol{\Phi}_2)$ and matrix $\boldsymbol{A}$ has two nontrival real different eigenvalues. If

$$\boldsymbol{v}^T(\varepsilon, \theta)\boldsymbol{T}(\theta) = 0 \tag{32}$$

then $\exists \beta \in R^1$ makes

$$\lim_{\varepsilon \to 0} \left[(\boldsymbol{A} - \beta \boldsymbol{I}) \begin{pmatrix} \cos\theta \\ \sin\theta \end{pmatrix} \right] = \boldsymbol{0} \tag{33}$$

where $\boldsymbol{I}$ is unit matrix of 2×2.

Proof: The Tayor expansion of $\boldsymbol{v}(\boldsymbol{y}^* + \Delta \boldsymbol{y})$ at $\boldsymbol{y}^*$ is

$$\boldsymbol{v}(\boldsymbol{y}^* + \Delta \boldsymbol{y}) = \boldsymbol{v}(\boldsymbol{y}^*) + D\boldsymbol{v}(\boldsymbol{y}^*)\Delta \boldsymbol{y} + o\|\Delta \boldsymbol{y}\| \tag{34}$$

Since

$$\boldsymbol{v}(\boldsymbol{y}^*) = \boldsymbol{0}, \qquad \Delta \boldsymbol{y} = \varepsilon(\boldsymbol{\Phi}_1 \cos\theta + \boldsymbol{\Phi}_2 \sin\theta)$$

Therefore,

$$\boldsymbol{v}(\boldsymbol{y}^* + \Delta \boldsymbol{y}) = D\boldsymbol{v}(\boldsymbol{y}^*)\varepsilon(\boldsymbol{\Phi}_1 \cos\theta + \boldsymbol{\Phi}_2 \sin\theta) + o(\varepsilon) \tag{35}$$

Substituting Eqs. (16) and (35) into Eq. (32), we get

$$\left(-\boldsymbol{\Phi}_1^T \sin\theta + \boldsymbol{\Phi}_2^T \cos\theta\right) D\boldsymbol{v}(\boldsymbol{y}^*)\varepsilon(\boldsymbol{\Phi}_1 \cos\theta + \boldsymbol{\Phi}_2 \sin\theta) + o(\varepsilon) = 0 \tag{36}$$

Dividing Eq. (36) by ε, we have

$$\left(-\boldsymbol{\Phi}_1^T \sin\theta + \boldsymbol{\Phi}_2^T \cos\theta\right) D\boldsymbol{v}(\boldsymbol{y}^*)(\boldsymbol{\Phi}_1 \cos\theta + \boldsymbol{\Phi}_2 \sin\theta) + O(\varepsilon) = 0 \tag{37}$$

Let

$$\boldsymbol{z} = \begin{pmatrix} z_1 \\ z_2 \end{pmatrix} = \begin{pmatrix} \cos\theta \\ \sin\theta \end{pmatrix}$$

$$b_{ij} = \boldsymbol{\Phi}_i^T D\boldsymbol{v}(\boldsymbol{y}^*)\boldsymbol{\Phi}_j, \qquad i, j = 1, 2 \tag{38}$$

Then

$$\boldsymbol{A} = \begin{pmatrix} b_{11} & b_{12} \\ b_{21} & b_{22} \end{pmatrix}$$

Substituting Eq. (38) into (37), as $\varepsilon \to 0$, we get

$$\boldsymbol{z}^T \begin{pmatrix} b_{21} & -b_{11} \\ b_{22} & -b_{12} \end{pmatrix} \boldsymbol{z} = 0$$

that is,

$$\boldsymbol{z}^T \boldsymbol{A}^T \begin{pmatrix} -z_2 \\ z_1 \end{pmatrix} = 0 \tag{39}$$

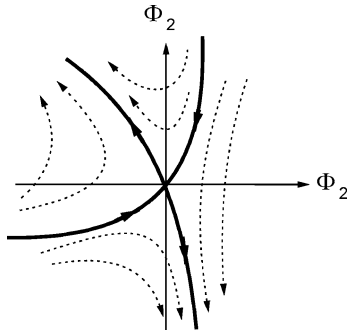

Fig. 4 Streamline distribution of $\boldsymbol{p}$.

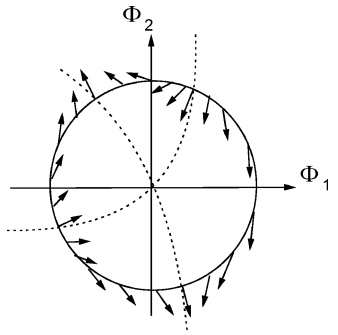

Fig. 5 Direction distribution of $\boldsymbol{p}$ along the circle.

Considering that

$$\begin{pmatrix} z_1 \\ z_2 \end{pmatrix} \neq \boldsymbol{0}$$

in Eq. (38) and that matrix $\boldsymbol{A}$ has two nontrival real different eigenvalues, we can obtain from Eq. (39) that $\exists \beta \in R^1$ makes $\boldsymbol{Az} = \beta \boldsymbol{z}$, that is,

$$\lim_{\varepsilon \to 0} \left[(\boldsymbol{A} - \beta \boldsymbol{I}) \begin{pmatrix} \cos\theta \\ \sin\theta \end{pmatrix} \right] = 0$$

□

According to Theorem 4, under Eq. (31), vector

$$\begin{pmatrix} \cos\theta \\ \sin\theta \end{pmatrix}$$

is parallel to one of eigenvectors of matrix $\boldsymbol{A}$ as $\varepsilon \to 0$. Thus, the approximate bifurcation directions determined by Eq. (31) converge to the exact bifurcation direction $\boldsymbol{u}^1$ or $\boldsymbol{u}^2$ in Eq. (11).

The streamline distribution of $\boldsymbol{p}$ near bifurcation point is shown in Fig. 4. Solid lines denote the projection of each solution curve on the null space, and the dotted lines denote the streamline of $\boldsymbol{p}$. The direction distribution of $\boldsymbol{p}$ along the circle is drawn in Fig. 5, where the dotted lines denote the projection of the two solution curves on the null space or on the tangential plane.

V. Stability Criterion

If an elastic body is discretized by FEM, it becomes a finite dimension system. Thus, the state of the system can be determined by a group of variables $\boldsymbol{x} \in R^n$, where n is the dimension number of the system. The total potential energy can be written as $\Pi = \Pi(\boldsymbol{x}, \lambda)$, where $\lambda \in R^1$ is a parameter, for example, λ can be a load factor. Let $\boldsymbol{F}(\boldsymbol{x}, \lambda) = (\partial \Pi / \partial x_i)$, $i = 1, 2, \ldots, n$, then $D_x\boldsymbol{F} = (\partial^2 \Pi / \partial x_i \partial x_j)$, $i, j = 1, 2, \ldots, n$ where $D_x\boldsymbol{F}$ is the Hessian matrix of the system. In nonlinear FEM, $D_x\boldsymbol{F}$ is the total tangent stiffness matrix. Because matrix $D_x\boldsymbol{F}$ is a symmetrical matrix, there is a nonsingular matrix $\boldsymbol{B}$ that makes $\boldsymbol{B}^T(D_x\boldsymbol{F})\boldsymbol{B} = \mathrm{diag}(d_1, d_2, \ldots, d_n)$. In this paper, $(d_1, d_2, \ldots, d_n) \neq 0$ is considered.

According to the Lagrange–Dirichlet theorem, total potential energy is the minimum if and only if the system is in stable equilibrium. Thus, the system is in stable equilibrium if and only if

1) $\boldsymbol{F}(\boldsymbol{x}, \lambda) = 0$, which is Eq. (1), and 2) the Hessian matrix is positive definite, that is, matrix $D_x\boldsymbol{F}$ is a positive definite matrix, in which $d_1, d_2, \ldots, d_n$ is all positive. Therefore, the numerical procedure for the equilibrium stability criterion is that if $d_i > 0$, $i = 1, 2, \ldots, n$, then the equilibrium is stable and if $\exists i \in (1, 2, \ldots, n)$ makes $d_i \le 0$, then the equilibrium is unstable.

VI. Numerical Procedure

A. Direction of Vector $\boldsymbol{v}$

In the pseudo-arc-length continuation, the direction of $\boldsymbol{v}$ must be given before the Euler prediction. In Eq. (6), the length of $\boldsymbol{v}$ is of no significance for Euler prediction. In fact, the length of $\boldsymbol{v}$ cannot be calculated accurately by the numerical method when n is a large number. However, the direction of $\boldsymbol{v}$ can be calculated accurately by the numerical method.

Because rank $(D_x\boldsymbol{F}, D_\lambda\boldsymbol{F}) = \text{rank}(D_x\boldsymbol{F}) = n$ at nonsingular point $\boldsymbol{y}$, we can transform matrix $D\hat{\boldsymbol{F}}(\boldsymbol{y})$ into a diagonal matrix by primary transformation:

$$D\hat{\boldsymbol{F}}(\boldsymbol{y}) \Rightarrow \begin{pmatrix} d_1 & & & & r_1 \\ & \ddots & & & \vdots \\ & & d_k & & r_k \\ & & & \ddots & \vdots \\ & & & & d_n\, r_n \end{pmatrix} \tag{40}$$

It is obvious that

$$\prod_{j=1}^{n} d_j \neq 0$$

at nonsingular point $\boldsymbol{y}$. According to the definition of $\boldsymbol{v}$ in Eq. (5), we have components of $\boldsymbol{v}$:

$$v_i = (-1)^n r_i \prod_{j \neq i} d_j \qquad (i = 1, \ldots, n)$$

$$v_{n+1} = (-1)^{n+1} \prod_{j=1}^{n} d_j \tag{41}$$

Because n is a large number (generally $n > 1000$), the error in the numerical results in Eq. (41) is very great. Thus, we divide Eq. (41) by

$$(-1)^{n+1} \left| \prod_{j=1}^{n} d_j \right|$$

$$\bar{v}_i = -\frac{r_i}{d_i} \operatorname{sgn}\left(\prod_{j=1}^{n} d_j \right) \qquad (i = 1, \ldots, n)$$

$$\bar{v}_{n+1} = \operatorname{sgn}\left(\prod_{j=1}^{n} d_j \right) \tag{42}$$

The direction of vector $\bar{\boldsymbol{v}} = (\bar{v}_1, \bar{v}_2, \ldots, \bar{v}_n, \bar{v}_{n+1})$ is the same as or opposite to the direction of vector $\boldsymbol{v}$. Although n is a large number in Eq. (42), numerical calculation of vector $\bar{\boldsymbol{v}}$ is accurate. Thus, the unit vector of $\boldsymbol{v}$, namely, $\boldsymbol{\tau} = \pm\bar{\boldsymbol{v}}/\|\bar{\boldsymbol{v}}\|$, can be calculated accurately. In the numerical procedure, we calculate $\boldsymbol{\tau}$ instead of $\boldsymbol{v}$.

B. Searching for Pitchfork Bifurcation Point

If $\boldsymbol{a}$ and $\boldsymbol{b}$ are nonsingular points on the solution curve, matrix $D\hat{\boldsymbol{F}}(\boldsymbol{a})$ and $D\hat{\boldsymbol{F}}(\boldsymbol{b})$ can be transformed into a diagonal matrix in Eq. (40). Here d_i^a and r_i^a, $i = 1, 2, \ldots, n$ denote elements of the diagonal matrix in Eq. (40) at point $\boldsymbol{a}$; d_i^b and r_i^b, $i = 1, 2, \ldots, n$, denote elements of the diagonal matrix in Eq. (40) at point $\boldsymbol{b}$.

Based on Theorem 1, inequality $\boldsymbol{\tau}^T(\boldsymbol{a})\boldsymbol{\tau}(\boldsymbol{b}) < 0$ is a criterion for the existence of a pitchfork bifurcation point on the solution curve. For simple-bifurcation point, inequality $\boldsymbol{\tau}^T(\boldsymbol{a})\tau(\boldsymbol{b}) < 0$ is equivalent to that $\exists k \in (1, 2, \ldots, n)$, which makes $d_k^a\, d_k^b < 0$, $r_k^a r_k^b < 0$ and $d_j^a d_j^b > 0$, $r_j^a r_j^b > 0$, $j = 1, 2, \ldots, k-1, k+1, \ldots, n$.

The range $(\boldsymbol{a}, \boldsymbol{b})$ is reduced by the golden section until $\|\boldsymbol{a} - \boldsymbol{b}\|$ is small enough. Then, an approximate bifurcation point $\boldsymbol{y}^{**}$ is obtained. At the same time, number k is recorded in the code.

C. $\boldsymbol{\Phi}_1$ and $\boldsymbol{\Phi}_2$ for Null Space $N[D\hat{\boldsymbol{F}}(\boldsymbol{y}^{**})]$

At approximate point $\boldsymbol{y}^{**}$ for the simple-bifurcation point, it should be that rank $[D\hat{\boldsymbol{F}}(\boldsymbol{y}^{**})] = n - 1$. Thus, we can transform matrix $D\hat{\boldsymbol{F}}(\boldsymbol{y}^{**})$ into a diagonal matrix by primary transformation except for column k, that is,

$$D\hat{\boldsymbol{F}}(\boldsymbol{y}^{**}) \Rightarrow \begin{pmatrix} d_1 & & d_{1,k} & & r_1 \\ & \ddots & \vdots & & \vdots \\ & & d_{k-1}\; d_{k-1,k} & & r_{k-1} \\ & & d_{k,k} & & r_k \\ & & d_{k+1,k}\; d_{k+1} & & r_{k+1} \\ & & \vdots & \ddots & \vdots \\ & & d_{n,k} & & d_n\, r_n \end{pmatrix} \tag{43}$$

where $d_{k,k}$ and r_k are close to zero.

Let $\boldsymbol{\Phi} = (\varphi_1, \ldots, \varphi_{n+1})$ and $D\hat{\boldsymbol{F}}(\boldsymbol{y}^{**})\boldsymbol{\Phi} = 0$. Considering rank $[D\hat{\boldsymbol{F}}(\boldsymbol{y}^{**})] = n - 1$, we know that only two elements in $\boldsymbol{\Phi}$ are independent. Letting $\varphi_k = 1$ and $\varphi_{n+1} = 0$, we have one base vector $\boldsymbol{\Phi}_1$ for null space $N[D\hat{\boldsymbol{F}}(\boldsymbol{y}^{**})]$ by the following equation:

$$\begin{pmatrix} d_1 & & & & & \\ & \ddots & & & & \\ & & d_{k-1} & & & \\ & & & d_{k+1} & & \\ & & & & \ddots & \\ & & & & & d_n \end{pmatrix} \begin{pmatrix} \varphi_1 \\ \vdots \\ \varphi_{k-1} \\ \varphi_{k+1} \\ \vdots \\ \varphi_n \end{pmatrix} = - \begin{pmatrix} d_{1k} \\ \vdots \\ d_{k-1k} \\ d_{k+1k} \\ \vdots \\ d_{nk} \end{pmatrix} \tag{44}$$

Letting $\varphi_k = 0$ and $\varphi_{n+1} = 1$, we have another base vector $\boldsymbol{\Phi}_2$ for null space $N[D\hat{\boldsymbol{F}}(\boldsymbol{y}^{**})]$ by the following equation:

$$\begin{pmatrix} d_1 & & & & & \\ & \ddots & & & & \\ & & d_{k-1} & & & \\ & & & d_{k+1} & & \\ & & & & \ddots & \\ & & & & & d_n \end{pmatrix} \begin{pmatrix} \varphi_1 \\ \vdots \\ \varphi_{k-1} \\ \varphi_{k+1} \\ \vdots \\ \varphi_n \end{pmatrix} = - \begin{pmatrix} r_1 \\ \vdots \\ r_{k-1} \\ r_{k+1} \\ \vdots \\ r_n \end{pmatrix} \tag{45}$$

By making vector $\boldsymbol{\Phi}_1$ and $\boldsymbol{\Phi}_2$ perpendicular to each other and unit, we have a null space approximately at the bifurcation point, that is, $N[D\hat{\boldsymbol{F}}(\boldsymbol{y}^*)] = \text{span}(\boldsymbol{\Phi}_1, \boldsymbol{\Phi}_2)$, where $\boldsymbol{\Phi}_1^T\boldsymbol{\Phi}_2 = 0$ and $\|\boldsymbol{\Phi}_1\| = \|\boldsymbol{\Phi}_2\| = 1$.

D. Searching Bifurcation Direction

As a suitable ε is given, $g(\theta) = \boldsymbol{\tau}^T(\varepsilon, \theta)\boldsymbol{T}(\theta)$ is considered to be an objective function. According to Theorem 3, the zero point of $g(\theta)$ is searched numerically in $\theta \in [-\pi, \pi]$. First, the range $[-\pi, \pi]$ is divided into several subranges so that there is only one zero point of $g(\theta)$ at best in each subrange. Second, the value of $g(\theta)$ at two endpoints of each subrange is calculated. Third, there is a zero point of $g(\theta)$ in a subrange if the sign of $g(\theta)$ at the two endpoints of the subrange is different. Fourth, the zero point of $g(\theta)$ is searched by bisection in the subrange. Finally, by substituting the zero point θ into $\boldsymbol{\Phi}_1 \cos\theta + \boldsymbol{\Phi}_2 \sin\theta$, we obtain an approximate bifurcation direction $\Delta\boldsymbol{y} = \boldsymbol{\Phi}_1 \cos\theta + \boldsymbol{\Phi}_2 \sin\theta$.

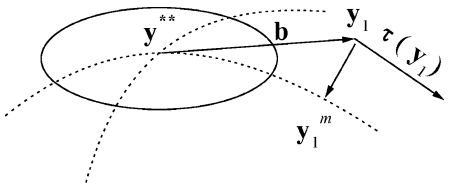

Fig. 6 Procedure of branch switching in space R^3.

According to Theorem 3 in Sec. III and Theorem 4 in Sec. IV, there should be four zero points of $g(\theta)$ on $\theta \in [-\pi, \pi]$. These four zero points correspond to four bifurcation directions. One couple corresponds to the tangential direction of the initial solution curve and another couple corresponds to the tangential direction of the branch solution curve as shown in Fig. 5. Obviously, the calculation of $g(\theta)$ does not need the information of derivative of $D_x\boldsymbol{F}$.

E. Branch Switching

After one bifurcation direction is selected in the four directions and a suitable arc-length step Δs is given, Euler prediction can be done at bifurcation point $\boldsymbol{y}^{**}$

$$\boldsymbol{y}_1 = \boldsymbol{y}^{**} + (\boldsymbol{\Phi}_1 \cos\theta + \boldsymbol{\Phi}_2 \sin\theta)\Delta s \tag{46}$$

Tangential vector $\boldsymbol{\tau}(\boldsymbol{y}_1)$ can be calculated by Eq. (42). By Newton correction,

$$\boldsymbol{y}_1^0 = \boldsymbol{y}_1$$

$$\boldsymbol{y}_1^m = \boldsymbol{y}_1^{m-1} - \begin{bmatrix} D\hat{\boldsymbol{F}}(\boldsymbol{y}_1) \\ \boldsymbol{\tau}^T(\boldsymbol{y}_1) \end{bmatrix}^{-1} \begin{bmatrix} \hat{\boldsymbol{F}}\left(\boldsymbol{y}_1^{m-1}\right) \\ 0 \end{bmatrix}, \qquad m = 1, 2, \ldots \tag{47}$$

The sequence $\boldsymbol{y}_1^0, \boldsymbol{y}_1^1, \boldsymbol{y}_1^2, \ldots$, converges to $\boldsymbol{y}_1^m$ on the solution curve corresponding to the bifurcation direction being selected. This branch solution curve is traced starting at $\boldsymbol{y}_1^m$. For the parameter space R^3, the scheme of the branch-switching procedure is shown in Fig. 6. The dotted lines are solution curves. The vector from $\boldsymbol{y}^{**}$ to b, which is a zero point of $g(\theta)$ on the circle, is an approximate bifurcation direction. Point $\boldsymbol{y}_1^m$, which is a convergent point by Newton correction starting at Euler prediction point $\boldsymbol{y}_1$, is a point on one of the solution curves.

F. Stability of Equilibrium

By primary transformation, matrix $D_x\boldsymbol{F}$ is transformed into the diagonal matrix $\mathrm{diag}(d_1, d_2, \ldots, d_n)$ in Eq. (40). According to criterion of stability in Sec. V, we can see that, if $d_1, d_2, \ldots, d_n$ are all positive, the equilibrium is stable and if $d_1, d_2, \ldots, d_n$ are not all positive, the equilibrium is unstable.

VII. FEM Simulation for Mode Jumping of a Square Plate

The described numerical procedure for branch switching has been inserted into a general FEM code by the authors. As a numerical example, the mode jumping of a square plate, in which there are many pitchfork bifurcations, is simulated by the improved FEM code. Many researchers[1–20] have long been interested in the mode jumping of rectangular plates.

A. Model of Square Plate

In Ref. 2, the mode-jumping experiments were conducted on several square plates, in postbuckling, which have different thicknesses and initial imperfections. The initial central deflection of each plate is listed in Table 1. The edge length of these plates is $l = 300$ mm as shown in Fig. 7.

The plates are considered under two types of clamped support boundary conditions, which are close to the boundary conditions in the experiments in Ref. 2.

Boundary condition 1:

$$x = 0: \qquad u = v = w = w_{,x} = 0$$

Table 1 Central initial deflection of each plate

	Model			
Property	1	2	3	4
Thickness h, mm	1.0	2.0	2.0	1.5
Initial defection, mm	0.315	0.076	0.048	——

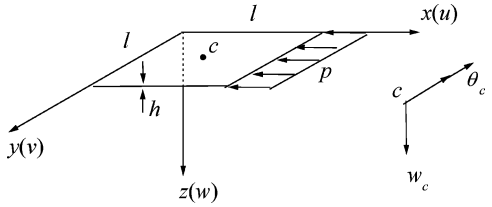

Fig. 7 Square plate loaded by uniaxial compression p.

$$x = l: \qquad v = w = w_{,x} = 0, \qquad N_x = -p$$

$$y = 0, l: \qquad w = w_{,y} = 0, \qquad N_y = 0 \tag{48}$$

Boundary condition 2:

$$x = 0: \qquad u = v = w = w_{,x} = 0$$

$$x = l: \qquad v = w = w_{,x} = 0, \qquad N_x = -p$$

$$y = 0, l: \qquad v = w = w_{,y} = 0 \tag{49}$$

The Poisson ratio is $\nu = 0.3$ and Young's modulus is E. Here w_c is the deflection at the central point $c(l/2, l/2, 0)$, θ_c is $w_{,y}$ at central point c, $\lambda = pl^2/D\pi^2$ is the load factor, which is the parameter in Eq. (1), and $D = Eh^3/12(1 - \nu^2)$ is the bending stiffness of the plate.

B. Numerical Results

Under boundary condition 1 in Eq. (48), the numerical results of a perfect plate corresponding to model 2 and model 3 in Table 1 are interpreted as follows. The solution curve is traced from starting point, at which load factor $\lambda = 0$ and $\boldsymbol{x} = 0$ in Eq. (1). The load-deflection curve under boundary condition 1 in Eq. (48) is shown in Fig. 8. The solid line and the dotted line denote stable and unstable equilibrium, respectively. Points 1, B1, and C1 are the pitchfork bifurcation points, at which a branch solution curve appears.

As shown in Fig. 8, the branch solution curve at point 1 is curve 1, 2, 3, and curve 1, A2. The branch solution curve at point B1 is curve B1, B2, B3, ..., and the branch that is the symmetry part of curve B1, B2, B3, ... For clarity, the symmetry branch of B1, B2, B3, ..., is not shown in Fig. 8. The branch solution curve at point C1 is curve C1, C2, C3, ..., and the symmetry part of branch C1, C2, C3, ... Similarly, for clarity the symmetry branch of C1, C2, C3, ..., is not shown in Fig. 8.

Deformation of the plate corresponding to each solution branch is shown in Figs. 9–11. Deformations corresponding to branch 0, 1, 2, 3 and branch 5, 6, 7, 8 are stable. The symmetry part of the two branches is stable, too. Deformations corresponding to the solution curve 0, 1, 2, 3 and branch 5, 6, 7, 8, ..., can be observed in the experiment.

The physical significance of the two stable branches is presented as follows. When $\lambda < \lambda_1$, corresponding to curve 0–1, the plate remains in a plane that is stable. Load factor λ_1 is the Euler critical load. When $\lambda = \lambda_1$, a new solution branch 1–2–3 appears at point 1 in Fig. 8. On this branch, the plate buckles for the first time. The buckling deformation corresponding to point 2 is shown in Fig. 9. The load increases till point 3, at which $\lambda = \lambda_2$. The plate is in a postbuckling state with a half-wave in the load direction, which is observed in the experiment of Ref. 2. This buckling deformation may be called the first buckling state.

Numerical and experimental results of Euler critical load λ_1 are listed in Table 2. The value in parentheses is the apparent stress and

the other values are the modified values considering errors in the experiment.[2]

In Fig. 8, a limit point (tangential bifurcation point) appears as load reaches the load corresponding to point 3. There are two types of equilibrium. One is the first buckling state corresponding to point 3. Another is the second buckling state, with one buckling wave in the load direction corresponding to point 7, as shown in Fig. 9. Because point 3 is a limit point, the first buckling state corresponding to point 3 is a critical state, which is an unstable equilibrium. Because point 7 is on branch 5, 6, 7, 8, . . . , where the equilibrium is stable, the second buckling state corresponding to point 7 is stable. Thus, the plate jumps from equilibrium at point 3 to equilibrium at point 7 as load increases. In other words, the plate can jump abruptly from the first buckling state to the second buckling state. This is the mode jumping of a plate that is observed in experiment.[1,2] Point 3 is called the second bifurcation point, and the load corresponding to the second bifurcation point is called the second critical load. Factor λ_2 is the second critical load factor in Fig. 8. Numerical and experimental results of the second critical load factor λ_2 are compared in Table 3.

If the load decreases after the load exceeds the second critical load, the unloading path is different from the loading path. In Fig. 8, the equilibrium path indicated by the dotted arrow is the unloading path. As the load decreases to point 5, the mode jumping occurs in the unloading process, in which the number of buckling wave changes abruptly from one to one-half. Equilibrium corresponding to point 5 can jump to equilibrium corresponding to point 2 on branch 1, 2, 3, . . . , or equilibrium corresponding to point A2 on branch 1, A2, ... Although the equilibrium corresponding to point 2 and point A2 is the first buckling state, the deflection corresponding to point 2 and point A2 is the opposite. Deformation of the two types of buckling state is shown in Fig. 9. There are two possible mode jumpings: one is that point 5 jumps to point 2; another is that point 5 jumps to point A2. Among the two possible mode jumpings, it depends on the initial disturbance at point 5 which kind of mode jumping will occur. The critical load factor at point 5 is listed in Table 4. For models 2 and 3 in Table 1, the deflection of the first buckling state during loading is opposite to the deflection of the first buckling state during unloading in the experiment.[2]

The deformations on branches B1, B2, B3, . . . , and C1, C2, C3, . . . , in Fig. 8 are shown in Figs. 10 and 11, respectively. The equilibrium on the two branches is unstable. In other words, we cannot observe the deformations in Figs. 10 and 11.

C. Mode Jumping Under Double Symmetry Boundary Condition

The second bifurcation point is the limit point under boundary condition 1 in Eq. (48) and boundary condition 2 in Eq. (49), where the boundary condition on $x = 0$ is not the same as that on $x = l$. If

Table 2 Euler critical load λ_1

Model	Imperfect plate, experiment[2]	Perfect plate, numerical results[a]		
		Boundary 1	Boundary 2	Boundary 3
1	8.21 (8.81)	9.53	8.03	——
2	8.22 (8.82)			
3	8.44 (9.04)	9.53	8.03	9.53

[a]This paper.

Table 4 Critical load factor λ of mode-jumping during unloading, model 3[a]

Method	Imperfect plate	Perfect plate
Experiment[2]	(12.10)	
Numerical[b]		
Boundary 1		13.51
Boundary 2		15.28
Boundary 3		12.53

[a]Point 5, Fig. 8. [b]This paper.

Table 3 Second critical load factor λ_2

Model	Imperfect plate, experiment[2]	Perfect plate, experiment[2]	Perfect plate, numerical results[a]		
			Boundary 1	Boundary 2	Boundary 3
1	19.48 (21.41)	——	16.78	17.72	——
2	12.50 (13.62)	——	16.67	17.71	17.46
3	13.87 (15.02)	——			
4	——	14.98(16.55)	16.81	17.75	——

[a]This paper.

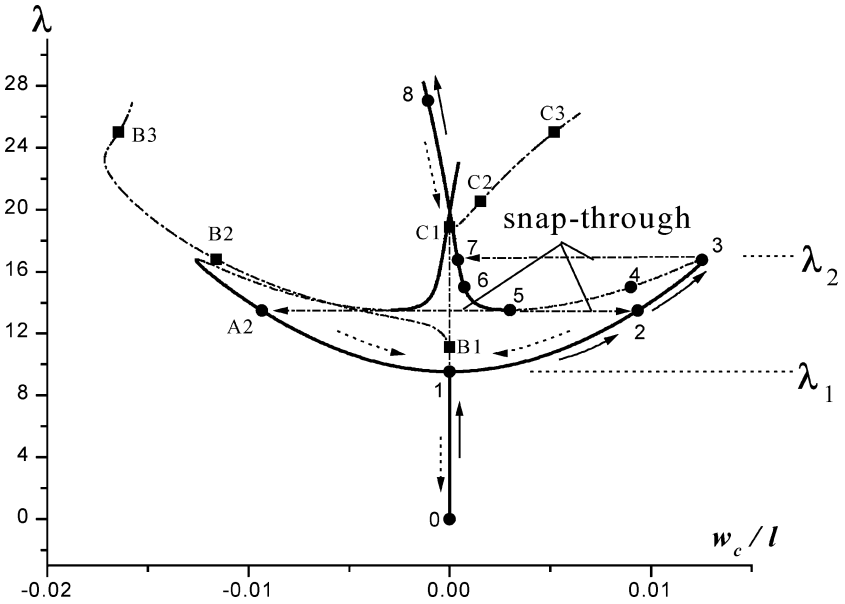

Fig. 8 Load-deflection curve under boundary condition 1 in Eq. (48).

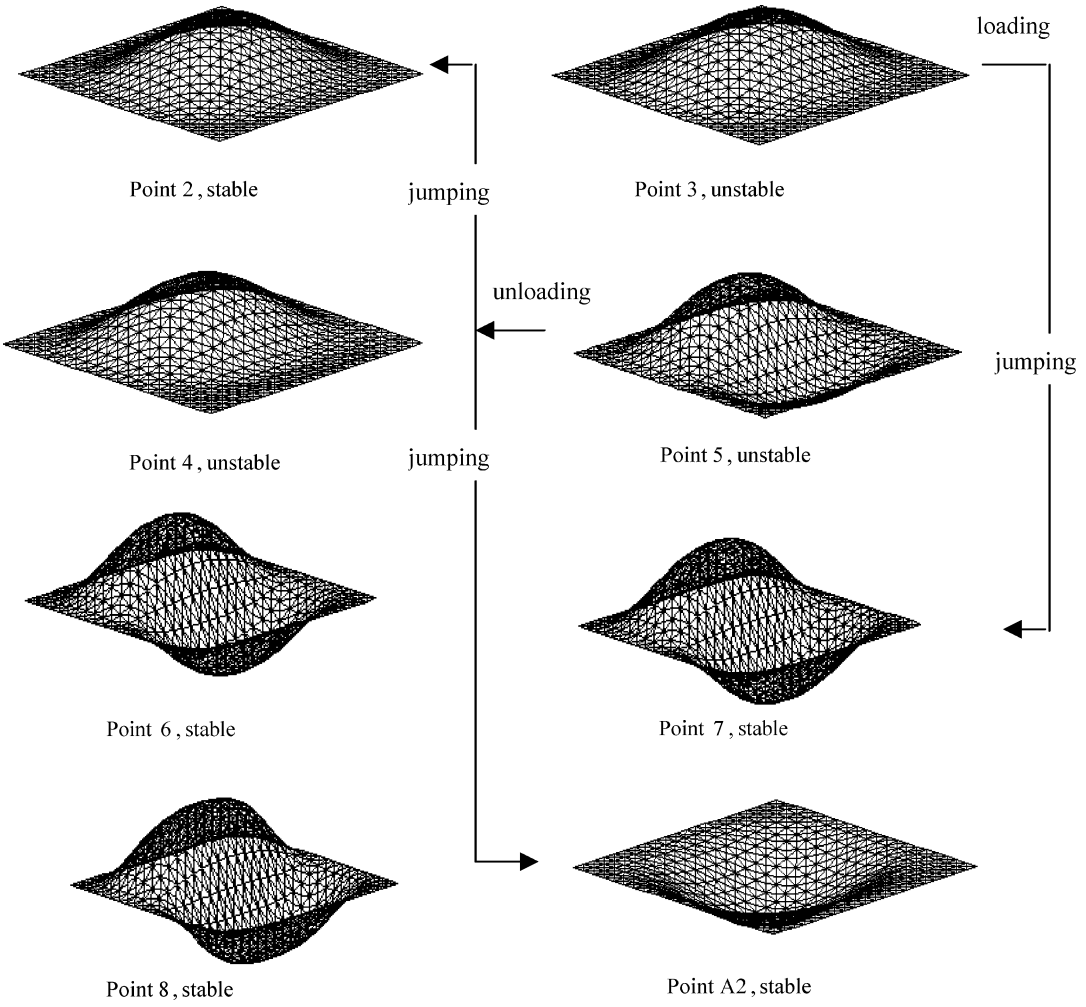

Fig. 9 Deformation corresponding to branch 1, 2, 3, . . . , and 1, A2 in Fig. 8.

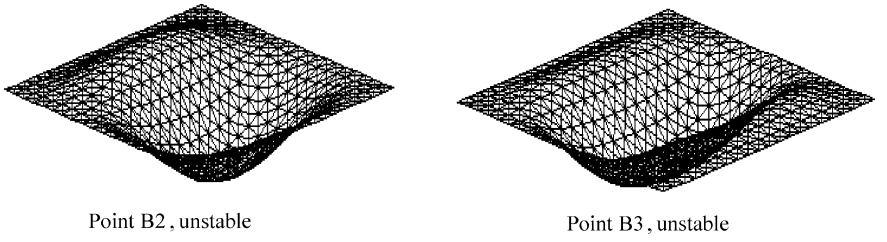

Fig. 10 Deformation corresponding to branch B1, B2, B3, . . . , in Fig. 8.

the boundary condition is the double symmetry boundary condition, in which the boundary condition on $x = 0$ is the same as that on $x = l$ and the boundary condition on $y = 0$ is the same as that on $y = l$, the second bifurcation is a pitchfork bifurcation. For example, boundary condition 3 in Eq. (50) is a type of double symmetry boundary condition.

Boundary condition 3:

$$\begin{aligned} x = 0, l: &\qquad v = w = w_{,x} = 0, &\qquad N_x = -p \\ y = 0, l: &\qquad w = w_{,y} = 0, &\qquad N_y = 0 \\ x = l/2 &\qquad y = 0, l: &\qquad u = 0 \end{aligned} \tag{50}$$

The numerical results of model 3 under boundary condition 3 are shown in Figs. 12–20. Because of the symmetry of the group of solution curves, one–quarter of the solution curves is shown in Fig. 12. Solid lines and dotted lines denote stable and unstable equilibrium, respectively. Arrows denote loading or unloading paths. Points 1, 3, C1, C2, D1, D2, E1, and G1 in Fig. 12 are pitchfork bifurcation points. Deformations corresponding to each solution curve are shown in Figs. 13–20.

In loading, the mode jumping occurs at point 3 in Fig. 12, where the equilibrium is a critical state, that is, the equilibrium corresponding to point 3 can jump to the equilibrium corresponding to point C3. The plate jumps from deformation with a half buckling wave to deformation with one buckling wave. Deformations before and after the mode jumping in loading are shown in Figs. 13 and 16, respectively. The load factor corresponding to point 3 is the second critical load factor λ_2. Numerical results of λ_2 are presented in Table 3. After the mode jumping, the load can increase along branch C3, C4, C5, . . . , where there is one buckling wave.

If the load decreases along branch C5, C4, C3, . . . , the mode jumping occurs at point C2, where the equilibrium is a critical

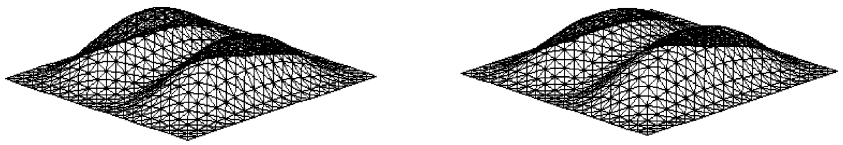

Point C2 , unstable Point C3 , unstable

Fig. 11 Deformation corresponding to branch C1, C2, C3, . . . , in Fig. 8.

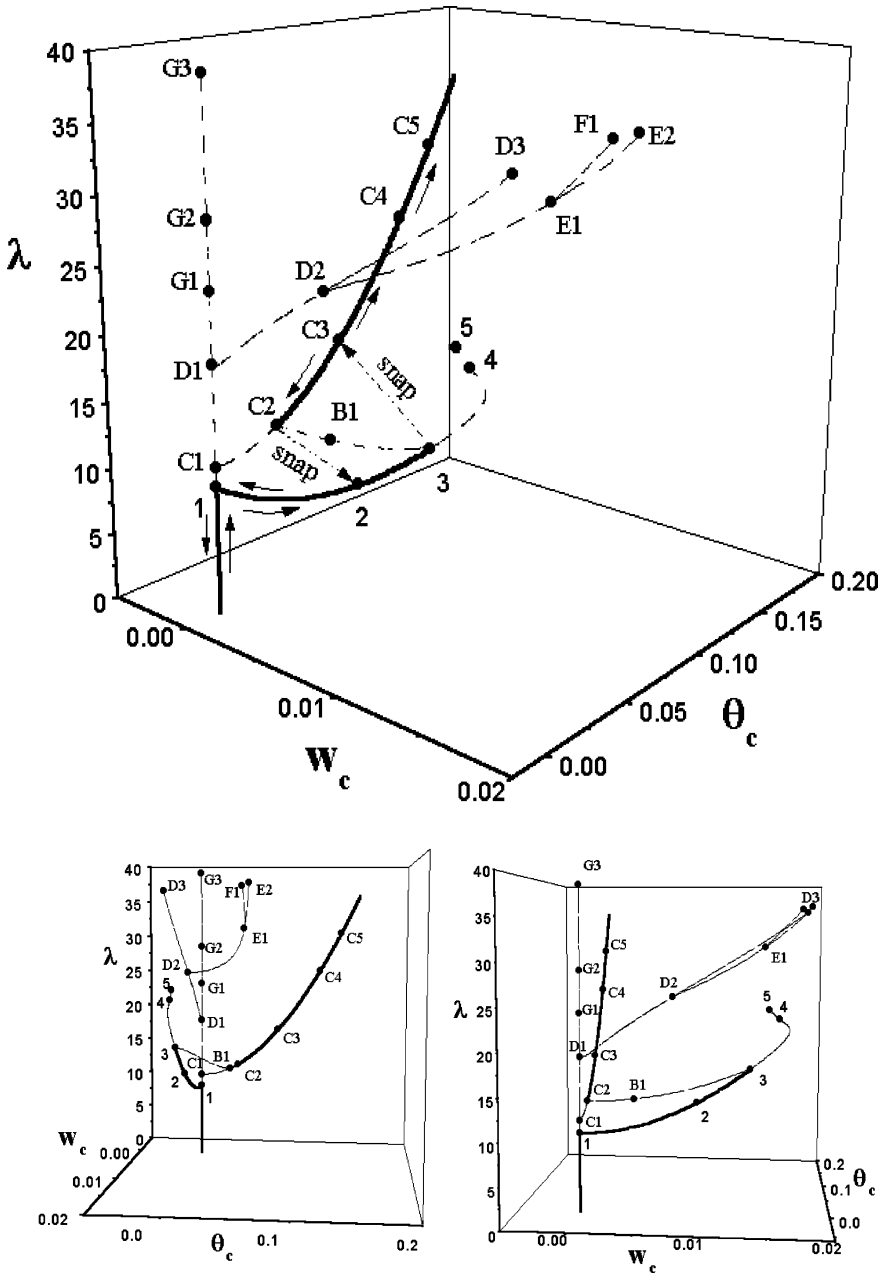

Fig. 12 Load-deflection curve under boundary 3.

state. The plate jumps from the deformation with one buckling wave to deformation with one-half buckling wave. The equilibrium corresponding to point C2 jumps to the equilibrium corresponding to point 2 in Fig. 12. Deformation of the plate before and after the mode jumping in unloading is shown in Figs. 16 and 13, respectively. The critical load factor λ corresponding to point C2 in Fig. 12 is listed in Table 4. After the mode jumping in unloading, the load can decrease along branch 2, 1. As the load decreases to Euler load at point 1, the plate resumes its original plane.

Deformations on branch 3, 4, 5, . . . ; branch 3, B1, C2, . . . ; branch D1, D2, D3, . . . ; branch D2, E1, E2, . . . ; branch E1, F1, . . . ; and branch G1, G2, G3, . . . , in Fig. 12 are shown in Figs. 14–20. Deformations of the plate on these branches are all unstable.

D. Some Instructions

For the square plate in Fig. 7, the geometrically nonlinear triangle plate element is used and the element number is $40 \times 40 = 1600$. For model 3 under condition 3, at the pitchfork bifurcation point 3 in

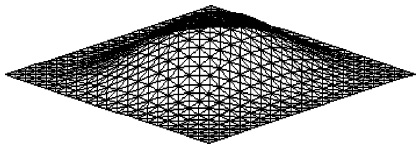

a) Point2, stable

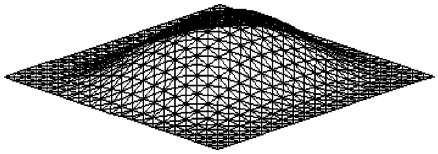

b) Point3, unstable

Fig. 13 Deformation on branch 1, 2, 3.

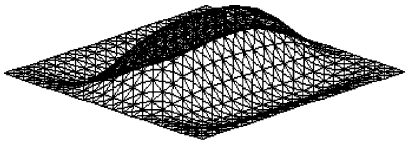

Point 5, unstable

Fig. 14 Deformation on branch 3, 4, 5.

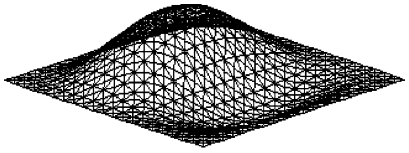

Point B1, unstable

Fig. 15 Deformation on branch 3, B1, C2.

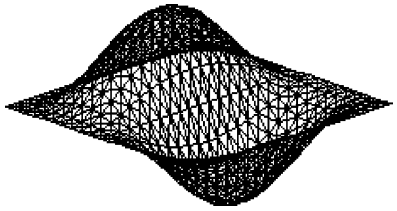

a) Point C2, unstable

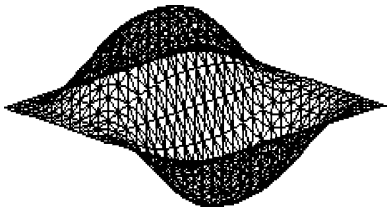

b) Point C3, stable

Fig. 16 Deformation on branch C1, C2, ...

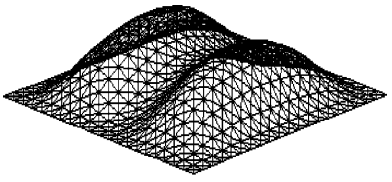

Fig. 17 Deformation on branch D1, D2, D3, . . . , unstable.

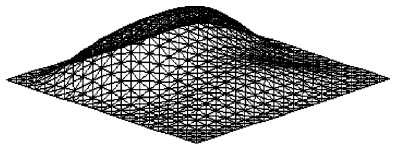

Fig. 18 Deformation on branch E1, E2, . . . , unstable.

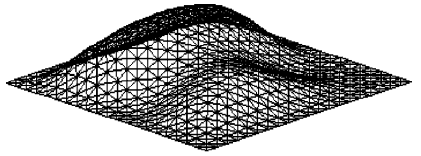

Fig. 19 Deformation on branch E1, F1, . . . , unstable.

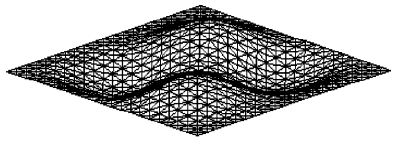

Fig. 20 Deformation on branch G1, G2, G3, . . . , unstable.

Fig. 12, ε is chosen to be the same order as the arc length $s_k - s_{k-1}$ in Eq. (6). For model 3 under condition 3, to trace the solution curve on C3, C4, C5 in Fig. 12, the relative error in each arc-length step reduces to less than 0.001 after three to five iterations for Newton correction.

For the perfect plate corresponding to model 3 under condition 1, it takes about 4-h CPU time with a Pentium II to obtain the load-deflection curves in Fig. 8. For model 3 under condition 3, it takes about 6-h CPU time with a Pentium II to obtain the load-deflection curves in Fig. 12.

The procedure in this paper has been inserted into the general nonlinear FEM code ADINA by the authors.

VIII. Conclusions

A numerical approach to pitchfork bifurcation direction is proposed for branch switching. This approach has the following properties:

1) It is suitable for bifurcation calculation of high-dimension problems. The degrees of freedom here is greater than 4000.

2) It is suitable for a general FEM code because the direction of new solution branch is determined without the information of derivatives of tangent stiffness matrix. Also, it is easy to insert the approach into a general FEM code.

3) It is a general approach because it is suitable for bar element, beam element, plate element, shell element, and so on.

4) This approach has a mathematical foundation, and the geometrical concept in the parameter space R^{n+1}.

5) Because CPU time on bifurcation direction is the time of calculation on the tangential vector, the CPU time of the branch switching here is not much longer than that of solving the total tangent stiffness equation.

In addition, the numerical procedure for the stability criterion is easy to insert into a general FEM code.

The improved code has been used to simulate the mode jumping of a square plate. The following points were indicated by the numerical results:

1) The solution of von Kármán equation of a plate has complicated bifurcation near the second critical load. For the square plate, two types of singular points, limit point and simple-pitchfork bifurcation point, appeared on the solution curves in the parameter space R^{n+1} under the double symmetry boundary condition 3.

2) These solution curves with stable equilibrium can simulate the first and the second buckling observed in the experiment.

3) The second bifurcation is the tangent bifurcation under the boundary conditions 1 and 2, where the boundary conditions on the two loading edges are not completely the same. The second

bifurcation is the simple-pitchfork bifurcation under boundary condition 3, where the boundary conditions of the two loading edges are the same. However, the mode jumping corresponding to the two types of bifurcation is the same physically because it is a jump from an unstable critical equilibrium to a stable equilibrium.

4) The numerical results of the second critical load are identical with the experimental results.

Acknowledgments

The authors acknowledge support from the National Science Foundation of the People's Republic of China through Grant 90205007 and the Science Foundation of Northern Jiaotong University through Grants TJ2002J0180 and PD-227. The authors gratefully acknowledge advice from J. K. Wu and K. F. Huang.

References

[1]Stein, M., "Loads and Deformations of Buckled Rectangular Plates," NASA TR, R-40, 1959.

[2]Uemura, M., and Byon, O., "Secondary Buckling of A Flat Plate Under Uniaxial Compression, Part II: Analysis of Clamped Plate by FEM and Comparison with Experiment," *International Journal of Non-Linear Mechanics*, Vol. 13, No. 1-A, 1978, pp. 1–14.

[3]Berger, M. S., "On von Kármán's Equations and the Buckling of a Thin Plate I: the Clamped Plate," *Communications on Pure and Applied Mathematics*, Vol. 20, No. 4, 1967, pp. 687–719.

[4]Schaeffer, D., and Golubitsky, M., "Boundary Conditions and Mode Jumping in the Buckling of a Rectangular Plate," *Communications in Mathematical Physics*, Vol. 69, 1979, pp. 209–236.

[5]Bauer, L., and Rriss, E. L., "Nonlinear Buckling of Rectangular Plates," *Journal of the Society for Industrial and Applied Mathematics*, Vol. 13, No. 3, 1965, pp. 603–626.

[6]Supple, W. J., "Changes of Waveform of Plate in the Post-Buckling Range," *International Journal of Solids and Structures*, Vol. 6, 1970, pp. 1243–1258.

[7]Stroebel, G. J., and Warner, W. H., "Stability and Secondary Bifurcation for von Kármán Plates," *Journal of Elasticity*, Vol. 3, 1973, pp. 185–202.

[8]Nakamura, T., and Uetani, K., "The Secondary Buckling and Post-Secondary Buckling Behavior of Rectangular Plates," *International Journal of Mechanical Sciences*, Vol. 21, No. 5, 1979, pp. 265–286.

[9]Matkowsky, B. J., Putnick, L. J., and Reiss, E. L., "Secondary States of Rectangular Plates," *SIAM Journal on Applied Mathematics*, Vol. 38, 1980, pp. 38–51.

[10]Ikeda, K., and Nakazawa, M., "Bifurcation Hierarchy of a Rectangular Plate," *International Journal of Solids and Structures*, Vol. 35, No. 7–8, 1998, pp. 593–671.

[11]Stoll, F., "Analysis of the Snap Phenomenon in Buckled Plates," *International Journal of Non-Linear Mechanics*, Vol. 29, No. 2-B, 1994, pp. 123–138.

[12]Everal, P. R., and Hunt, G. W., "Mode Jumping in the Buckling of Struts and Plates: A Comparative Study," *International Journal of Non-Linear Mechanics*, Vol. 35, 2000, pp. 1067–1079.

[13]Everal, P. R., and Hunt, G. W., "Arnold Tongue Predictions of Secondary Buckling in Thin Elastic Plates," *Journal of Mechanics and Physics of Solids*, Vol. 47, 1999, pp. 2187–2206.

[14]Chien, C. S., Kuo, Y. J., and Mei, Z., "Bifurcation of the von Kármán Equations with Robin Boundary Conditions," *Computers and Mathematics with Applications*, Vol. 38, 1999, pp. 85–112.

[15]Stoll, F., "An Implementation of Solution Strategies for the Analysis of Complex Non-Linear Equilibrium Behavior," *International Journal of Non-Linear Mechanics*, Vol. 29, No. 2, 1994, pp. 109–122.

[16]Carnoy, E. G., and Hughes, T. J. R., "Finite Element Analysis of Secondary Buckling of a Flat Plate Under Uniaxial Compression," *International Journal of Non-Linear Mechanics*, Vol. 18, No. 2, 1983, pp. 167–175.

[17]Gervais, J. J., Oukit, A., and Pierre, R., "Finite Element Analysis of the Buckling and Mode Jumping of a Rectangular Plate," *Dynamics and Stability*, Vol. 12, No. 3, 1997, pp. 161–185.

[18]Wohlever, J. C., "Some Computational Aspects of a Group Theoretic Finite Element Approach to the Buckling and Post-Buckling Analyses of Plates and Shells-of-Revolution," *Computer Methods in Applied Mechanics and Engineering*, Vol. 170, 1999, pp. 373–406.

[19]Eriksson, A., Costin Pacoste, C., and Zdunek, A., "Numerical Analysis of Complex Instability Behavior Using Incremental-Iterative Strategies," *Computer Methods in Applied Mechanics and Engineering*, Vol. 179, 1999, pp. 265–305.

[20]Stoll, F., and Olson, S. E., "Finite Element Investigation of the Snap Phenomenon on Buckled Plates," *Stability Analysis of Plates and Shells, A Collection of Papers in Honor of Dr. Manuel Stein*, compiled by N. F. Knight Jr., NASA CP-1998-206280, pp. 435–444.

[21]Riks, E., Rankin, C. C., and Brogan, F. A., "On The Solution of Mode Jumping Phenomena in Thin-Walled Shell Structures," *Computer Methods in Applied Mechanics and Engineering*, Vol. 136, No. 1-2, 1996, pp. 59–92.

[22]Keller, H. B., *Lectures on Numerical Methods in Bifurcation Problems*, Springer-Verlag, New York, 1987.

[23]Riks, E., "An Incremental Approach to Solution of Snapping and Buckling Problems," *International Journal of Solids and Structures*, Vol. 15, 1979, pp. 529–551.

[24]Allgower, E. G., and Georg, K., *Numerical Continuation Methods*, Vol. 13, Springer Series in Computational Mathematics, Springer, Berlin, 1990.

[25]Riks, E., "Some Computational Aspects of the Stability Analysis of Nonlinear Structures," *Computer Methods in Applied Mechanics and Engineering*, Vol. 47, No. 3, 1984, pp. 219–259.

S. Saigal
Associate Editor